Available online at www.sciencedirect.com
ScienceDirect
Journal of Catalysis 246 (2007) 40–51
JOURNAL OF CATALYSIS
www.elsevier.com/locate/jcat

Selective hydrogenation of acetylene in the presence of ethylene on zeolite-supported bimetallic catalysts

Wei Huang [a], John R. McCormick [b], Raul F. Lobo [a], Jingguang G. Chen [a,*]

[a] *Department of Chemical Engineering, University of Delaware, Newark, DE 19711, USA*
[b] *Department of Materials Science and Engineering Center for Catalytic Science and Technology (CCST), University of Delaware, Newark, DE 19711, USA*

Received 20 June 2006; revised 12 October 2006; accepted 11 November 2006
Available online 21 December 2006

Abstract

Novel catalysts were synthesized by supporting Pd-based bimetallic catalysts on Na^+-exchanged β-zeolites to achieve higher selectivity for the hydrogenation of acetylene in the presence of ethylene at room temperature. Batch reactor studies carried out using infrared spectroscopy show that Pd–Ag bimetallic catalysts have higher selectivity for acetylene hydrogenation in the presence of ethylene than either Pd or Ag monometallic catalysts. Kinetic modeling of the reaction data reveals significant differences in the hydrogenation rate constants and adsorption equilibrium constants. The influence of the Na^+-β-zeolite support is compared with traditional γ-Al_2O_3-supported catalysts. The Na^+-β-zeolite-supported catalysts exhibit higher selectivity than their γ-Al_2O_3 counterparts. Overall, zeolite-supported Pd–Ag bimetallic catalyst was found to have the highest selectivity of the catalysts studied.

Keywords: Hydrogenation; Acetylene; Ethylene; Pd–Ag; Pd–Ni; Bimetallic catalysts; Zeolite

1. Introduction

Ethylene is a crucial intermediate in many industrial reactions. One of the most important of these is ethylene polymerization. Ethylene is produced by thermal or catalytic cracking of higher hydrocarbons, which also generates impurities, such as acetylene, that can poison traditional polymerization catalysts. To prevent catalyst poisoning, the concentration of acetylene must be <5 ppm [1–4]. The typical method used in industry for reducing acetylene concentration is selective hydrogenation of acetylene using Pd catalysts [5–7]. Due to the poor selectivity at high acetylene conversion and oligomer formation during acetylene hydrogenation, the current commercial Pd-based catalysts have considerable room for improvement. The objective of the current work is to develop new catalysts by combining Pd-based bimetallic catalysts and zeolite supports to achieve higher selectivity for the selective hydrogenation of acetylene in a stream containing ethylene.

Previous studies [2,8–12] showed that acetylene hydrogenation produces ethylene, which is then hydrogenated to ethane. The initial steps of the reaction mechanism include dissociative adsorption of hydrogen on the catalyst surface. Acetylene and ethylene are also co-adsorbed on the catalyst before reaction. Addition of the first hydrogen atom to acetylene or ethylene is the rate-determining step [9–14]. Ethylene–acetylene hydrogenation is a classical case of a series-parallel reaction. The reaction is in series in terms of acetylene and ethylene but parallel with respect to hydrogen, which means there is no direct formation of ethane from acetylene [2,12]. The hydrogenation mechanisms can be written as

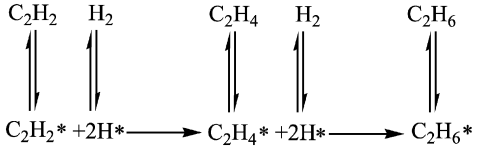

Zeolite-supported metal catalysts often show superior selectivity and activity in many reactions [15,16]. In zeolites, extra-framework cations can bind to the π face of a double

* Corresponding author.
E-mail address: jgchen@udel.edu (J.G. Chen).

0021-9517/$ – see front matter
doi:10.1016/j.jcat.2006.11.013

or triple carbon–carbon bond structure through a noncovalent force known as cation–π interaction [17,18]. The interaction can be considered an electrostatic attraction between a positive charge and the quadrupole moment of the π-bond. The interaction is usually strong and changes with cation identity. Alkenes generally are more polarizable than alkynes, yet show lower binding energies to cations [19] in the gas phase because of this π–quadruple interaction. One possible advantage of zeolite-supported catalyst is to use cation–π interactions to preferentially adsorb acetylene in an ethylene-rich environment, thus enhancing the local concentration of acetylene and achieving higher hydrogenation selectivity. To avoid blocking of the zeolite pores by metal particles and reaction byproducts, the preferred zeolite is expected to be a structure containing a multidimensional pore system with large pore apertures (12 rings). Two promising candidates are the zeolite Y or X (FAU) and the zeolite β (*BEA). We studied zeolite β in the present work.

A major challenge is that using preferential adsorption of acetylene to increase selectivity requires carrying out the experiments at relatively low temperatures. There is no distinguishable preferential adsorption at high temperatures, because the difference in adsorption equilibrium constants decreases exponentially with temperature. The bimetallic system is a plausible solution to achieve acceptable levels of low-temperature hydrogenation activity. Bimetallic catalysts also provide a method of tuning catalytic materials to obtain highly selective and highly active catalysts. Comparisons of recombinative desorption of H_2 and D_2 on the bimetallic and the corresponding monometallic surfaces have been studied previously [20–25]. The dissociative adsorption of H_2 on transition metal surfaces is a nonactivated process [26]; thus, the observation of a lower desorption temperature on bimetallic surfaces indicates that hydrogen atoms bind more weakly than on either of the parent metals. In principle, the presence of weakly bonded hydrogen atoms should favor low-temperature hydrogenation, as demonstrated for the hydrogenation of cyclohexene [21] and other alkenes [27]. Thus, in the current study, bimetallic catalysts are supported on the zeolites to potentially reduce the activation energy of the rate-determining hydrogenation step and simultaneously maintain the preferential adsorption of acetylene at low temperatures. Pd-based catalysts have shown superior selectivity and activity for the selective hydrogenation reaction [5–7]; thus a second metal, such as Ni or Ag, has been added to the Pd catalyst in an attempt to achieve higher selectivity and activity.

The primary objective of the current study is to synthesize and evaluate zeolite-supported Pd–Ni and Pd–Ag bimetallic catalysts for the selective hydrogenation of acetylene in the presence of ethylene. We performed batch reactor studies to confirm the novel and promising catalytic properties of zeolite-supported bimetallic catalysts compared with those supported on γ-Al_2O_3 and to those of monometallic catalysts. Furthermore, we performed kinetic modeling to provide a more quantitative comparison of the hydrogenation activity and selectivity of the various monometallic and bimetallic catalysts.

2. Experimental

2.1. Catalyst preparation

Supported catalysts were synthesized using Pd, Ni, and Ag supported on either γ-Al_2O_3 (Alfa-Aesar, 99.7%) or Na^+-exchanged β-zeolite support using the incipient wetness method [1–4]. The β-zeolite (SiO_2:Al_2O_3 = 25, Zeolyst Company) was originally obtained in its ammonia form. Before the addition of metal precursor, the zeolite was ion-exchanged twice with 500 mL of 0.01 M $NaNO_3$ solutions to obtain a Na^+-formed zeolite. After the ion-exchange process, the zeolite was washed with DI water and dried at 383 K. The γ-Al_2O_3 support was used as received.

The Pd–Ni bimetallic catalysts (Table 1) were prepared by co-impregnation using $Pd(NO_3)_2$ (Alfa-Aesar) and $Ni(NO_3)_2 \cdot xH_2O$ (Alfa-Aesar), whereas the Pd–Ag bimetallic catalysts were prepared by sequential impregnation using $Pd(NO_3)_2$ and then $AgNO_3$ (Alfa-Aesar), because of the low solubility of the Ag salts. The impregnated supports were dried in air overnight. The catalysts were then dried at 383 K for 5 h and calcined in air at 623 K for 6 h.

The dispersion of supported Pd and PdAg catalysts was determined by carbon monoxide (CO) chemisorption experiments, whereas the dispersion of supported Ni and PdNi catalysts was studied by hydrogen (H_2) chemisorption experiments to avoid the stoichiometric problem of CO–Ni. Pulse CO chemisorption/H_2 chemisorption experiments were carried out using an Altamira Instruments AMI-200ip. The catalysts were reduced in dilute hydrogen at 723 K for 1 h and cooled to room temperature in a helium/argon stream. Pulses of CO/H_2 in a helium/argon carrier gas were injected into the quartz reactor, and the signal was monitored by a thermal conductivity detector (TCD). The mean stoichiometry CO–XPd was determined according to the iterative method derived by Lambert et al. [28]: In brief, the starting value of X = 0.5 was chosen for CO–XPd, and a first value of Pd dispersion was calculated from the CO uptake. A polynomial function was fitted based on the table established by Joyal and Butt [29], who determined CO–XPd as a function of dispersion in Pd/SiO_2 catalysts. Using this fitted function, a new value of CO–XPd was determined corresponding to the precedent obtained dispersion value; this new value of CO–XPd was used to calculate a new value of dispersion. The iterative cycle was repeated until convergence. Using this iterative method, the values of CO–XPd were determined to be 0.62 for Pd/γ-Al_2O_3 and 0.69 for Pd/Na^+-β-zeolite; these values were used to determine the dispersion of the two Pd catalysts. According to the literature, pure Ag does not chemisorb CO [30–32]. Because in monometallic catalysts CO chemisorption

Table 1
Catalysts compositions in wt% on γ-Al_2O_3 and Na^+-β-zeolite

Support	Pd	Pd–Ni	Pd–Ag
γ-Al_2O_3	1.36	1.36, 0.75 Atomic ratio: 1:1	1.36, 1.38 Atomic ratio: 1:1
β-Zeolite	1.36	1.36, 0.75 Atomic ratio: 1:1	1.36, 1.38 Atomic ratio: 1:1

Table 2
Catalyst dispersion from CO or H_2 chemisorption measurements

Sample	CO chemisorption		H_2 chemisorption	
	Dispersion (%)	Uptake per gram catalyst	Dispersion (%)	Uptake per gram catalyst
Pd/γ-Al_2O_3	16.4	13.0		
Pd/β-zeolite	23.1	20.3		
PdAg/γ-Al_2O_3	14.2	13.6		
PdAg/β-zeolite	20.9	20.2		
PdNi/γ-Al_2O_3			11.3	14.4
PdNi/β-zeolite			12.4	15.9
Ni/γ-Al_2O_3			10.6	6.8
Ni/β-zeolite			11.6	7.4
Ag/γ-Al_2O_3	–	–	–	–
Ag/β-zeolite	–	–	–	–

occurs on Pd but not on Ag, it was assumed that on the surface of alloy particles in Pd–Ag bimetallic catalysts, CO chemisorption occurred only on Pd atoms [33,34], which was supported by Somanoto et. al. [31]. Results from our current study also confirmed no strong interaction between CO and Ag/γ-Al_2O_3 and Ag/β-zeolite. Therefore, the dispersion of Pd–Ag bimetallic catalysts was determined based on the assumption that CO adsorbed only on surface Pd atoms. The dispersions of the Pd–Ag catalysts were also determined using CO chemisorption. Balerna et al. found that Pd–Ag bulk alloys (0.5 wt% Pd and 0.6 wt% Ag) consist of a phase of almost pure Ag and another phase with similar Pd and Ag composition [35]. Because the stoichiometry of CO–XPd is 0.5 [29] for low-dispersed Pd and <1 for a Ag-rich Pd–Ag alloy [31], a mean stoichiometry of CO/Pd of 0.75 was assumed based on the average of 0.5–1 for the Pd–Ag catalysts in the current study.

The mean stoichiometry of H_2 chemisorption was assumed to be 0.5 on supported Ni catalysts [36,37] due to the dissociate adsorption of H_2 on transition metals [38]. In H_2 chemisorption analysis done to determine the dispersion of Pd catalysts at 28 °C, a stoichiometric number of 0.5 was also assumed [39]. Therefore, in the current study the dispersion of Ni and Pd–Ni catalysts was determined by H_2 chemisorption analysis assuming a stoichiometry of 0.5. Table 2 shows the metal dispersions on the corresponding catalysts.

2.2. Reaction rate measurements

Fourier transform infrared (FTIR) spectroscopy was used to examine the kinetics of the hydrogenation reactions. The IR experiments were performed using a stainless steel IR cell with of BaF_2 windows, which allowed in situ reduction of samples and spectroscopic measurements of surface species and gas-phase products in a batch reactor based on the design reported previously [40]. Spectra were recorded at room temperature with 4 cm^{-1} spectral resolution by collecting 128 scans for gas-phase and 512 scans for surface species using a Nicolet-510 FTIR spectrometer equipped with a MCT-A (mercury cadmium telluride) detector.

Powder catalysts samples of ∼22 mg were pressed onto a square tungsten mesh with a spot-welded K-type thermocouple to monitor the temperature. To remove water and other impurities the cell was evacuated to a pressure $<10^{-6}$ Torr at room temperature for 30 min and then reduced at 723 K in 30 Torr hydrogen for 30 min, which was followed by evacuation and a high-temperature flash (723 K) to remove any surface species generated during the reduction. The reduction cycle was repeated three times before performing IR experiments.

The gas-phase reaction products were monitored by recording gas-phase spectra every 60 s during the reaction. A mixture of 10% acetylene in 90% helium mixture (Matheson) was purified by passing it through a dry ice–acetone trap. The effects of purification were tested by comparing 60-Torr purified mixture and 60-Torr unpurified mixture; the latter showed trace amounts of acetone. Research-grade ethylene (Matheson) and hydrogen (Keen) were used without further purification. The IR cell was filled with 10-Torr 10% acetylene and 1-Torr ethylene. After equilibration and the formation of a stable baseline, 6-Torr H_2 was introduced to initiate reaction at room temperature, and the IR spectra were recorded. The concentrations of the three main species—acetylene, ethylene, and ethane—were determined by the classical least squares method using the C–H stretching vibrational features from 2600 to 3500 cm^{-1} [41].

3. Results

3.1. Calibration of gas-phase IR intensity

The concentrations of gas-phase C_2H_2, C_2H_4, and C_2H_6 in the IR cell were calibrated using the classical least squares method [41] with a 16-member training set. The Beer–Lambert law states that the absorbance is proportional to the concentration,

$$\mathbf{A} = \mathbf{KC}, \tag{1}$$

where $\mathbf{A}$ is the training set of absorbance matrix, $\mathbf{K}$ is the proportionality constant, and $\mathbf{C}$ is the matrix of component concentrations. The subscript "unknown" refers to the reaction data. The coefficient $\mathbf{K}$ can be calculated as

$$\mathbf{K} = \mathbf{AC}^{\mathrm{T}}\left[\mathbf{CC}^{\mathrm{T}}\right]^{-1}. \tag{2}$$

Therefore, an unknown mixture concentration can be predicted by

$$\mathbf{C}_{\mathrm{unknown}} = \left[\mathbf{K}^{\mathrm{T}}\mathbf{K}\right]^{-1}\mathbf{K}^{\mathrm{T}}\mathbf{A}_{\mathrm{unknown}}. \tag{3}$$

In our calibration, a set of 16 gas mixtures of varying but known ratios of acetylene, ethylene, and ethane were each recorded at room temperature using 128 scans and a 4-cm^{-1} spectral resolution. These 16 spectra formed the absorbance matrix $\mathbf{A}$. The concentration values were included in the matrix of component concentrations $\mathbf{C}$ in the corresponding order as the spectra were stored in matrix $\mathbf{A}$. The coefficient $\mathbf{K}$ was then calculated using Eq. (2).

The spectrum of an unknown sample was truncated from 3500 to 2600 cm^{-1}, and an automatic baseline correction was applied. The resulting spectrum was labeled $\mathbf{A}_{\mathrm{unknown}}$, and the concentration of the unknown spectrum was then calculated using Eq. (3).

3.2. Parameter fitting

The equilibrium constants for the adsorption of acetylene and ethylene and the dissociative adsorption of hydrogen are defined as K_1, K_2, and K_3, respectively; k_1 and k_2 are the rate constants for the hydrogenation of acetylene and ethylene, respectively. The rate-determining step is the addition of the first hydrogen atom to an adsorbed acetylene or ethylene molecule [9–14]. The equations are as follows:

$$C_2H_2 + {}^* \rightleftharpoons C_2H_2^* \quad K_1, \tag{4}$$

$$C_2H_4 + {}^* \rightleftharpoons C_2H_4^* \quad K_2, \tag{5}$$

$$H_2 + 2^* \rightleftharpoons 2H^* \quad K_3, \tag{6}$$

$$C_2H_2^* + H^* \rightarrow C_2H_3^* + {}^* \quad k_1, \tag{7}$$

and

$$C_2H_4^* + H^* \rightarrow C_2H_5^* + {}^* \quad k_2. \tag{8}$$

The rates of acetylene hydrogenation and ethylene hydrogenation can be written as

$$r_{C_2H_2} = -k_1\theta_{C_2H_2}\theta_H \tag{9}$$

and

$$r_{C_2H_4} = -k_2\theta_{C_2H_4}\theta_H + k_1\theta_{C_2H_2}\theta_H, \tag{10}$$

where $\theta_{C_2H_2}$ and $\theta_{C_2H_4}$ represent the surface coverage of acetylene and ethylene, respectively. Using Langmuir–Hinshelwood classical approximations, the rate can be defined as

$$r_{C_2H_2} = -\frac{dC_{C_2H_2}}{dt} = -\frac{k_1K_1\sqrt{K_3}P_{C_2H_2}\sqrt{P_{H_2}}}{(1 + K_1P_{C_2H_2} + K_2P_{C_2H_4} + \sqrt{K_3P_{H_2}})^2} \tag{11}$$

and

$$r_{C_2H_4} = -\frac{dC_{C_2H_4}}{dt} = \frac{k_1K_1\sqrt{K_3}P_{C_2H_2}\sqrt{P_{H_2}}}{(1 + K_1P_{C_2H_2} + K_2P_{C_2H_4} + \sqrt{K_3P_{H_2}})^2} - \frac{k_2K_2\sqrt{K_3}P_{C_2H_4}\sqrt{P_{H_2}}}{(1 + K_1P_{C_2H_2} + K_2P_{C_2H_4} + \sqrt{K_3P_{H_2}})^2}. \tag{12}$$

In addition, the rates of ethane generation and hydrogen consumption can be expressed as

$$r_{C_2H_6} = k_2\theta_{C_2H_4}\theta_H \tag{13}$$

and

$$r_{H_2} = -k_1\theta_{C_2H_2}\theta_H - k_2\theta_{C_2H_4}\theta_H. \tag{14}$$

Therefore,

$$r_{C_2H_6} = \frac{dC_{C_2H_6}}{dt} = \frac{k_2K_2\sqrt{K_3}P_{C_2H_4}\sqrt{P_{H_2}}}{(1 + K_1P_{C_2H_2} + K_2P_{C_2H_4} + \sqrt{K_3P_{H_2}})^2} \tag{15}$$

and

$$r_{H_2} = -\frac{dC_{H_2}}{dt} = -\frac{k_1K_1\sqrt{K_3}P_{C_2H_2}\sqrt{P_{H_2}}}{(1 + K_1P_{C_2H_2} + K_2P_{C_2H_4} + \sqrt{K_3P_{H_2}})^2} - \frac{k_2K_2\sqrt{K_3}P_{C_2H_4}\sqrt{P_{H_2}}}{(1 + K_1P_{C_2H_2} + K_2P_{C_2H_4} + \sqrt{K_3P_{H_2}})^2}. \tag{16}$$

For convenience, the rate constants for acetylene hydrogenation and ethylene hydrogenation can be lumped as

$$k_1^* = k_1K_1\sqrt{K_3} \tag{17}$$

and

$$k_2^* = k_2K_2\sqrt{K_3}. \tag{18}$$

The equations used by the fitting program are (11), (12), (15), and (16).

Because the FTIR spectrometer cannot detect gas-phase H_2, the initial concentration of hydrogen was estimated as six times the initial acetylene concentration based on the experimental parameters. The concentration of hydrogen during the reaction was then calculated based on the reaction stoichiometry. The hydrogen equilibrium constant was set at 0.56 cm^3/mol based on [42]. The kinetic parameters were then calculated using Eqs. (11), (12), (15), and (16). The fitting algorithm also depends on the initial guess values. However, despite the changes of those fitted parameters, the ratio of $\frac{k_1K_1}{k_2K_2}$, defined as the relative selectivity of acetylene hydrogenation (S), remains nearly constant with respect to the initial guess values.

3.3. Hydrogenation over γ-Al_2O_3-supported PdNi and PdAg catalyst

Fig. 1 compares the concentrations of gas-phase C_2H_2, C_2H_4, and C_2H_6 as a function of reaction time at room temperature (298 K) over three γ-Al_2O_3-supported catalysts, Pd, PdNi, and PdAg. The sharp decrease of the total mass balance at $t = 20$ min is due to the introduction of 6.0-Torr hydrogen and an unavoidable consequence of back-mixing into the dosing lines. Due to the presence of excess H_2, the final product of all reactions was ethane. Based on the reaction time, the PdAg/γ-Al_2O_3 exhibited the highest hydrogenation activity among the three γ-Al_2O_3-supported catalysts, followed by PdNi/γ-Al_2O_3 and then Pd/γ-Al_2O_3. The acetylene concentration decreased during the reaction while ethane concentration increased until all acetylene and ethylene were consumed. In contrast, the ethylene concentration remained nearly constant for PdAg/γ-Al_2O_3 until the acetylene was almost completely consumed. The ethylene concentration on the Pd and PdNi catalysts decreased from the beginning of the reaction, although the rate of decrease was accelerated after the complete consumption of acetylene. The fitted curves, using the equations described earlier, are compared with experimental data in Fig. 2. The equilibrium and rate constants, derived from the fitting and normalized per surface active site, are listed in Table 3.

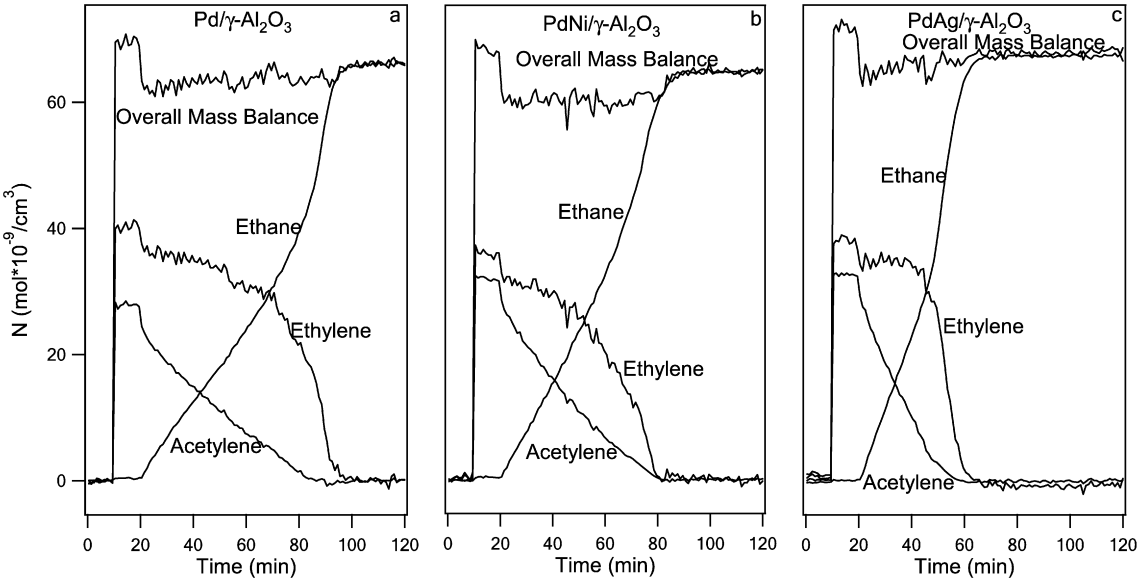

Fig. 1. Concentrations of gas-phase C_2H_2, C_2H_4, and C_2H_6 as a function of reaction time at room temperature on (a) Pd/γ-Al_2O_3, (b) PdNi/γ-Al_2O_3, and (c) PdAg/γ-Al_2O_3.

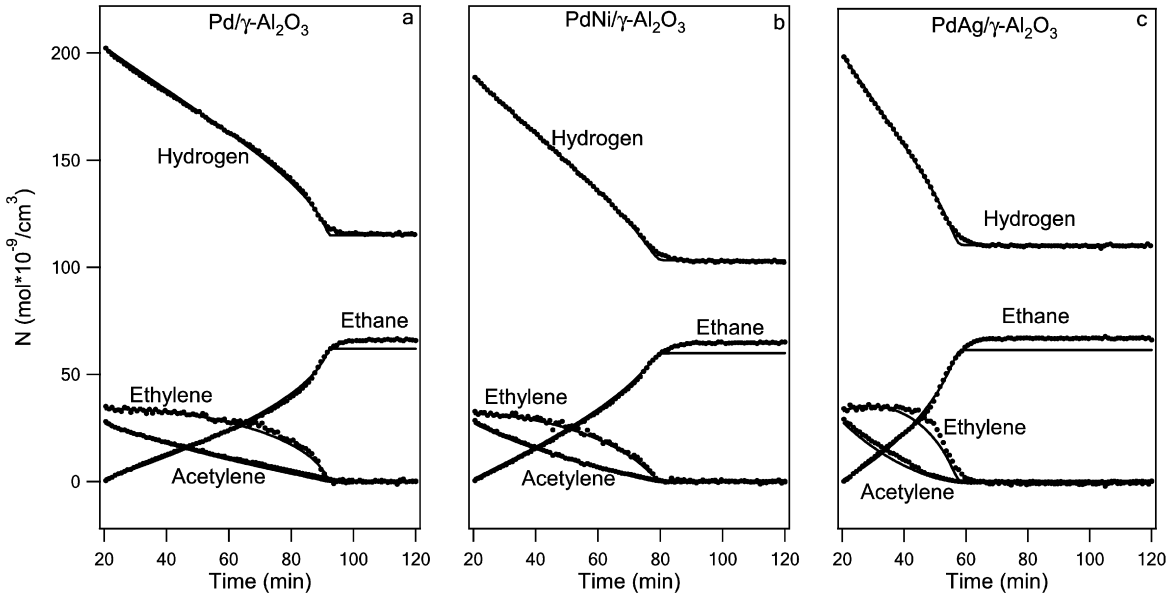

Fig. 2. Fitted concentrations of gas-phase C_2H_2, C_2H_4, and C_2H_6 on (a) Pd/γ-Al_2O_3, (b) PdNi/γ-Al_2O_3, and (c) PdAg/γ-Al_2O_3.

Table 3
Values of reaction rate constants and adsorption equilibrium constants fitted from experimental data

Catalysts	k_1 (min^{-1})	k_2 (min^{-1})	K_1 (cm^3/mol)	K_2 (cm^3/mol)	$S = (k_1/k_2)^*(K_1/K_2)$
Pd/γ-Al_2O_3	43.4±1.1	17.3 ± 1.8	1.9 ± 0.5	3.3 ± 0.3	1.4
PdNi/γ-Al_2O_3	33 ± 0.5	6.8 ± 0.1	0.6 ± 0.2	2.2 ± 0.5	1.3
PdAg/γ-Al_2O_3	35.2±1.0	16.4 ± 2.0	0.8 ± 0.2	0.8 ± 0.1	2.1
Pd/Na-β-zeolite	21.4±7.1	36.5 ± 0.9	2.7 ± 0.2	0.6 ± 0.3	2.6
PdNi/Na-β-zeolite	20.5±5.5	28.6 ± 1.3	3.3 ± 0.3	0.6 ± 0.2	3.9
PdAg/Na-β-zeolite	5.1±0.6	26.5 ± 5.9	5.2 ± 0.3	0.15 ± 0.05	6.8
Ag/γ-Al_2O_3[a]	5.5	0.8	0.4	6.1	–
Ni/Na-β-zeolite	4.8	2.0	3.1	1.8	–
Ag/Na-β-zeolite[a]	1.7	0.9	5.9	3.3	–

[a] Is calculated per gram of catalysts.

3.4. Hydrogenation over β-zeolite-supported catalysts

Fig. 3 compares the reaction kinetics of acetylene and ethylene hydrogenation over β-zeolite-supported Pd, PdNi, and PdAg catalysts at room temperature (298 K). The experiment conditions were the same as the γ-Al_2O_3-supported catalysts. Based on the reaction time, the β-zeolite-supported Pd and PdNi catalysts showed higher hydrogenation activities than those on the γ-Al_2O_3-supported Pd and PdNi catalysts, although the hydrogenation activity of PdAg/β-zeolite is lower than that of PdAg/γ-Al_2O_3. Similar to the γ-Al_2O_3-supported catalysts, the acetylene concentration decreased during the reaction while the ethane concentration increased until all of the acetylene and ethylene was consumed. However, on all of the β-zeolite-supported catalysts, the ethylene concentration initially increased and then began to decrease as the acetylene was consumed. The fitted curves are compared with experimental data in Fig. 4, and the kinetic parameters based on surface active sites are listed in Table 3.

The reactions on monometallic Ag/γ-Al_2O_3, Ni/γ-Al_2O_3, Ag/β-zeolite, and Ni/β-zeolite were also tested; these materials showed significantly lower hydrogenation activity (IR spectra not shown). The rate and equilibrium constants are compared in Table 3. Due to the low hydrogenation activity on Ni/γ-Al_2O_3, we were unable to find an acceptable solution to Eqs. (9)–(18) for this catalyst.

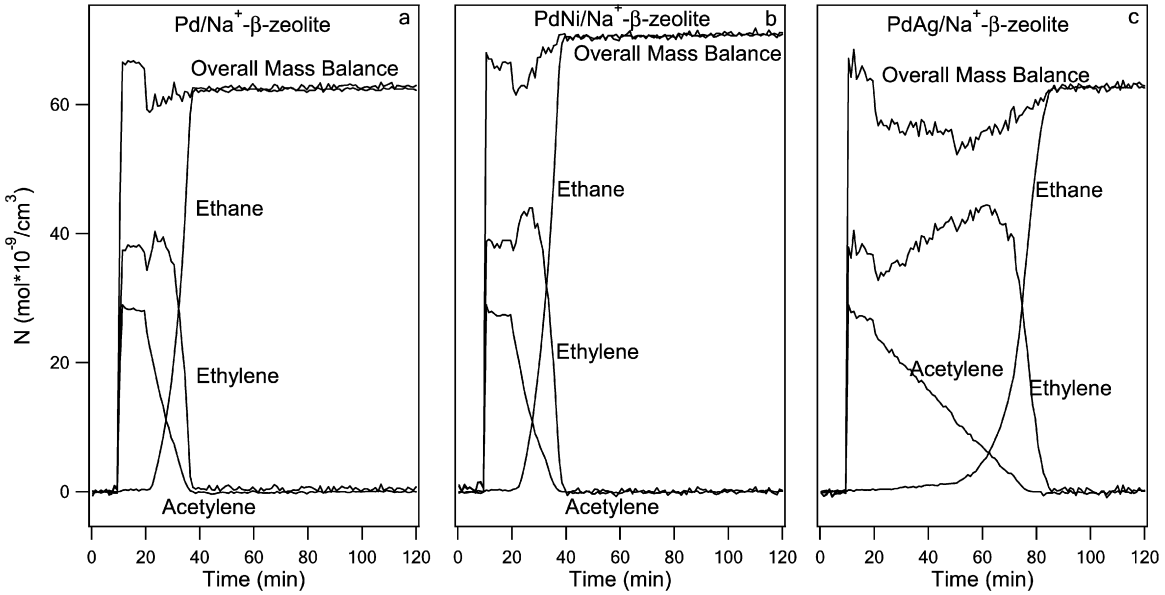

Fig. 3. Concentrations of gas-phase C_2H_2, C_2H_4, and C_2H_6 as a function of reaction time at room temperature on (a) Pd/Na^+-β-zeolite, (b) PdNi/Na^+-β-zeolite, and (c) PdAg/Na^+-β-zeolite.

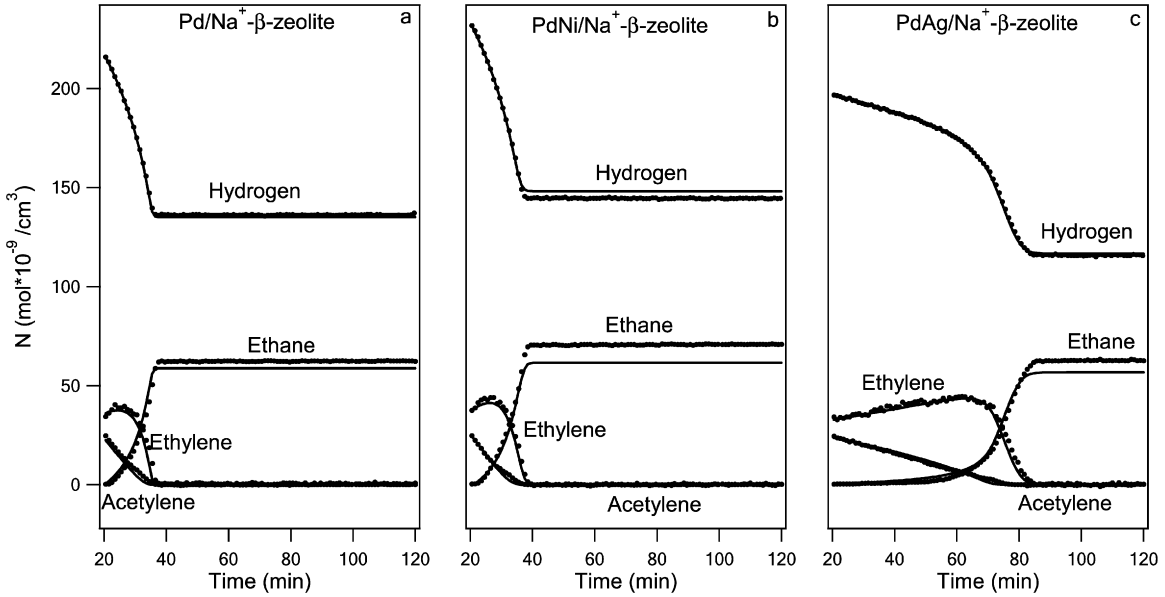

Fig. 4. Fitted concentrations of gas-phase C_2H_2, C_2H_4, and C_2H_6 on (a) Pd/Na^+-β-zeolite, (b) PdNi/Na^+-β-zeolite, and (c) PdAg/Na^+-β-zeolite.

3.5. Adsorbed species on different surfaces

Fig. 5 shows the IR spectra of the adsorbed mixture on γ-Al_2O_3-supported Pd, PdNi, and PdAg, the intensities of which are renormalized based on the number of active sites of metal. The IR spectra were recorded after exposing the catalysts to C_2H_2 and C_2H_4, followed by evacuation for ∼10 min. As found in previous vibrational studies [51,52], the adsorption and reaction of C_2H_2 and C_2H_4 can lead to a wide range of hydrocarbon fragments on surfaces, including π- and σ-bonded C_2H_2 and C_2H_4, and C_2 fragments, such as vinyl and ethylidyne. As a result, the vibrational assignment is rather complex. Table 4 provides a general assignment of vibrational features for the *sp*-, sp^2-, and sp^3-hybridized C_2H_x species. The expected frequencies for these species are also labeled in Fig. 5 for the main vibrational features. In the current study we are interested mainly in the relative concentrations of adsorbed species on the different catalyst surfaces. As shown in Fig. 5, the vibrational features for the CH, CH_2, and CH_3 functional groups are detected on Pd/γ-Al_2O_3 and PdNi/γ-Al_2O_3, indicating the formation of various surface C_2H_x species on the two catalysts. In contrast, the vibrational features on the PdAg/γ-Al_2O_3 surface are relatively weak and can be assigned to weakly π-bonded species. As reported in previous studies, π-bonded species are more easily hydrogenated [9,10], which is likely an important factor contributing to

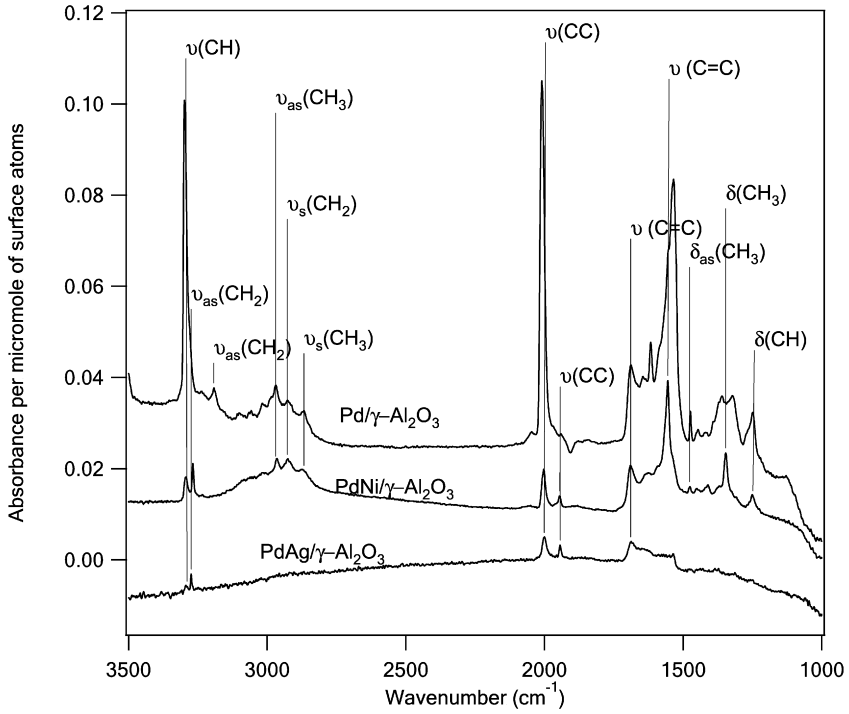

Fig. 5. IR spectra of mixture adsorption on (a) Pd/γ-Al_2O_3, (b) PdNi/γ-Al_2O_3, and (c) PdAg/γ-Al_2O_3.

Table 4
Assignment of IR spectra features of adsorbed species on catalysts supported on γ-Al_2O_3

Assignment	Pd/γ-Al_2O_3	PdAg/γ-Al_2O_3	PdNi/γ-Al_2O_3	Gas phase [64,65]	
				C_2H_2	C_2H_4
ν_{C-H}(≡C–H)	3298	3295	3293	3374	
				3287	
$\nu_{as}(CH_2)$	3192	3274	3266		
$\nu_{as}(CH_3)$	2969		2965		
$\nu_s(CH_2)$			2930		2960
$\nu_s(CH_3)$	2863 [66]		2872		
ν(C≡C)	2009	1999	2002	1974	
ν(C≡C) [67]		1945	1945		
ν(C=C) [67]	1688	1688	1689		1650
	1616	1649	1631		
ν(C=C) + $\delta(CH_2)$ [68]	1534	1534	1554		
$\delta_{as}(CH_3)$	1474		1472		
δ(CH)			1411	1355	
				1298	
$\delta(CH_3)$ (ethylidyne)	1320		1347		
δ(CH)	1245		1248		

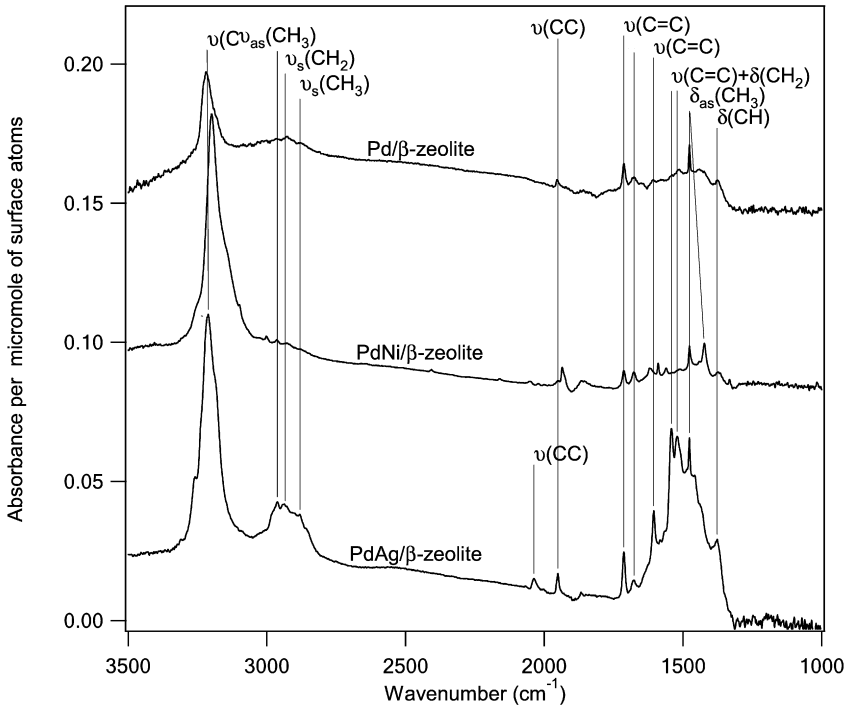

Fig. 6. IR spectra of mixture (C_2H_2 and C_2H_4) adsorption on (a) Pd/β-zeolite, (b) PdNi/β-zeolite, and (c) PdAg/β-zeolite.

Table 5
Assignment of IR spectra features of adsorbed species on catalysts supported on Na^+-β-zeolite

Assignment	Pd/β-zeolite	PdAg/β-zeolite	PdNi/β-zeolite
ν_{C-H}(≡C–H)	3204	3258	3200
		3212	
$\nu_{as}(CH_2)$	3180	3183	2999
$\nu_{as}(CH_3)$	2964	2964	2960
$\nu_s(CH_2)$	2930	2933	2926
$\nu_s(CH_3)$	2879	2875	2872
ν(C≡C)	1948	2034	1954
		1952	1936
ν(C=C)	1712	1712	1712
	1677	1674	1677
	1604	1608	1619
ν(C=C) + $\delta(CH_2)$	1573	1542	1561
	1515	1519	
$\delta_{as}(CH_3)$	1476	1476	1476
			1418
δ(CH)	1376	1372	1372
			1332

the higher hydrogenation activity on the PdAg/γ-Al_2O_3 catalyst.

Fig. 6 shows the adsorbed mixture (C_2H_2 and C_2H_4) on β-zeolite-supported Pd, PdNi, and PdAg, the intensities of which are renormalized based on the active sites of surface. The assignment of the frequencies is listed in Tables 5. Similar to Fig. 5, π-bonded species are observed on the zeolite-supported catalysts (Fig. 6). Based on the normalized IR intensities, the concentration of adsorbed species is higher on PdAg/β-zeolite than on Pd/β-zeolite and PdNi/β-zeolite. To further understand the competitive adsorption of C_2H_2 and C_2H_4, Fig. 7 shows the IR spectra after the adsorption of C_2H_2 and C_2H_4, of C_2H_2 only, and of C_2H_4 only. The comparison reveals that the adsorption of C_2H_4 is rather weak, as indicated by the relatively weak vibrational features after exposure of the catalyst to C_2H_4. In contrast, the adsorption of C_2H_2 is stronger, as demonstrated by the more intense vibrational features after exposure of the catalyst to C_2H_2. Although the IR spectrum of mixture adsorption is generally similar to that of C_2H_2, several additional features, particularly in the $\nu(CH_x)$ region, differ from those of either C_2H_2 or C_2H_4. More detailed IR studies are needed to clarify the origin of these intermediates, which are beyond the scope of the current paper.

4. Discussion

4.1. Effect of bimetallic formation

As shown in Table 3, PdAg/γ-Al_2O_3 has a higher selectivity for acetylene hydrogenation than Pd/γ-Al_2O_3 and PdNi/γ-Al_2O_3. The equilibrium constants for ethylene adsorption are larger on Pd/γ-Al_2O_3 and PdNi/γ-Al_2O_3 than on acetylene (Table 3). This indicates that the Pd/γ-Al_2O_3 and PdNi/γ-Al_2O_3 surfaces can adsorb ethylene more readily than acetylene. In comparison, on the PdAg/γ-Al_2O_3 catalyst, the equilibrium constants of ethylene and acetylene are comparable. Therefore, the selectivity to acetylene hydrogenation increases on PdAg/γ-Al_2O_3 mainly because the relative ratio of K_1/K_2 increases, which means that alloying Pd with Ag can help facilitate acetylene adsorption.

The calculated rate constant for acetylene hydrogenation is larger than that for ethylene hydrogenation on the three γ-Al_2O_3-supported catalysts, consistent with the hydrogenation barrier calculated in previous studies by Gislason et

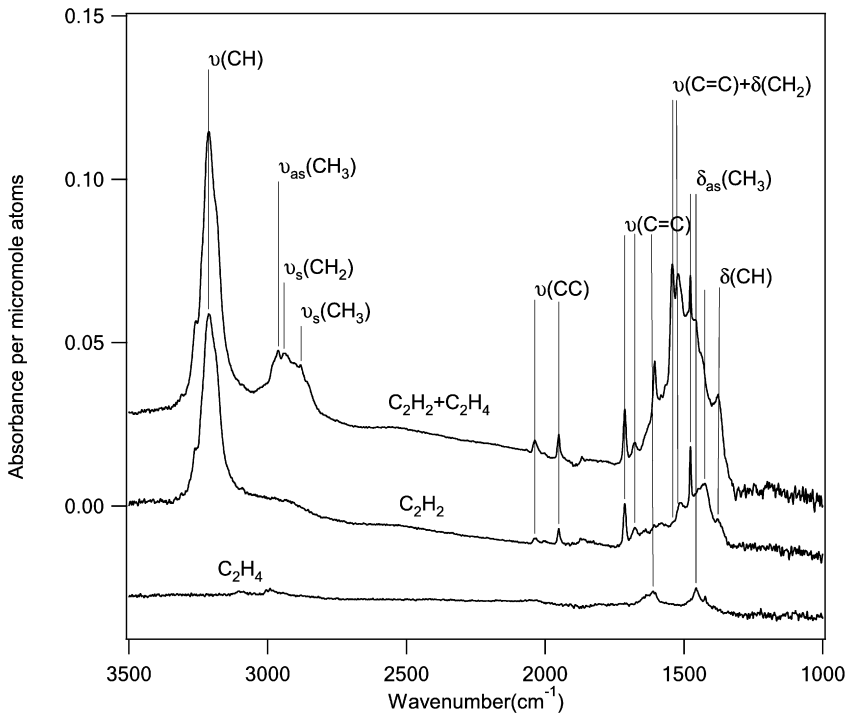

Fig. 7. IR spectra of adsorption on PdAg/β-zeolite, (a) mixture of C_2H_2 and C_2H_4, (b) C_2H_2 only, and (c) C_2H_4 only.

al. [43]. Our fitted data in Table 3 indicate that the rate constant of acetylene hydrogenation is smaller on PdAg/γ-Al_2O_3 than on Pd/γ-Al_2O_3, which is also consistent with literature reports indicating that alloying the Pd catalyst with Ag increases selectivity but reduces catalyst activity [43,44]. However, the higher ratio of equilibrium constants of acetylene over ethylene adsorption on PdAg/γ-Al_2O_3 results in an increase in the overall reaction rate in the batch reactor. From Eq. (11) and the constants given in Table 3, the rate of acetylene hydrogenation on Pd/γ-Al_2O_3 and PdAg/γ-Al_2O_3 can be written as

$$r_{C_2H_2} = -\frac{53.5\sqrt{K_3}P_{C_2H_2}\sqrt{P_{H_2}}}{(1+1.26P_{C_2H_2}+2.06P_{C_2H_4}+0.79\sqrt{K_3P_{H_2}})^2}$$

for Pd/γ-Al_2O_3

and

$$r_{C_2H_2} = -\frac{45.0\sqrt{K_3}P_{C_2H_2}\sqrt{P_{H_2}}}{(1+0.84P_{C_2H_2}+0.96P_{C_2H_4}+1.2\sqrt{K_3P_{H_2}})^2}$$

for PdAg/γ-Al_2O_3.

Although the numerator is larger for the rate on Pd/γ-Al_2O_3 than on PdAg/γ-Al_2O_3, the denominator can also become larger on Pd/γ-Al_2O_3 than on PdAg/γ-Al_2O_3, depending on the values of the partial pressures of reactants (e.g., the initial partial pressure of 1:1:6 for C_2H_2:C_2H_4:H_2). This in turn causes the overall rate on Pd/γ-Al_2O_3 to be smaller than that on PdAg/γ-Al_2O_3, as observed experimentally and shown in Fig. 1.

Alloying Pd with Ni weakens the acetylene and ethylene binding energies, as indicated by the decreased K_1 and K_2 values shown in Table 3. The reduced IR intensities for adsorbed species on PdNi/γ-Al_2O_3 compared with those on Pd/γ-Al_2O_3 supports this effect (Fig. 5). Our models show that alloying Ni reduces the rate constant, k, for ethylene hydrogenation more than for acetylene but has the opposite effect for the equilibrium constant, K (Table 3). These opposing changes might be responsible for the observation that the selectivity to acetylene hydrogenation is similar for PdNi/γ-Al_2O_3 and Pd/γ-Al_2O_3.

4.2. Effect of catalyst supports

The β-zeolite-supported Pd and PdNi catalysts show significantly higher activity than their γ-Al_2O_3-supported counterparts. We attribute this observation to the greater dispersion on β-zeolite support than on γ-Al_2O_3 support (Table 2), as well as to the reduced ethylene adsorption equilibrium constant (Table 3). It is interesting to point out that on the β-zeolite-supported catalysts, the equilibrium constant of ethylene is smaller than that of acetylene, opposite to what is observed on the γ-Al_2O_3-supported catalysts. We attribute this to the higher cation–π interactions between alkali metal Na^+ and the π-bond of acetylene than with ethylene. The strong interaction between the acetylene quadruple moment and Na^+ leads to an increase in the local concentration of acetylene and a decrease in the local ethylene concentration. The preferential adsorption of acetylene over ethylene leads to a higher selectivity for acetylene hydrogenation.

The rate constant for acetylene hydrogenation is lower on Pd/β-zeolite than on Pd/γ-Al_2O_3, whereas the rate constant for ethylene is higher on Pd/β-zeolite than on Pd/γ-Al_2O_3 (Table 3). A previous study [45] also found that the activity of acetylene hydrogenation decreases while the dispersion increases on the Pd/α-Al_2O_3. The β-zeolite-supported Pd shows higher dispersion than the γ-Al_2O_3-supported Pd (Table 2),

suggesting that the particle size of Pd clusters on β-zeolite is smaller than that on γ-Al_2O_3. Larger particle size favors the formation of palladium β-hydride [45,46], which plays an important role in the hydrogenation activity of acetylene.

Previous studies [47] have found that ethylene molecules preferentially adsorb in the di-σ configuration on the larger particles, whereas small particles favor the weakly bounded π ethylene molecules. Because the π-bonded ethylene is generally considered the intermediate hydrogenation species [48–50], smaller particles should promote the hydrogenation of ethylene over larger particles. These observations are a possible explanation of why the β-zeolite-supported Pd exhibits a higher rate constant for ethylene hydrogenation.

PdAg/β-zeolite exhibits the highest selectivity of the three β-zeolite-supported catalysts, followed by PdNi/β-zeolite and then Pd/β-zeolite. The higher selectivity of PdAg/β-zeolite is achieved by the selective adsorption of acetylene resulting from alloying with Ag on zeolite support. As shown in Table 3, the equilibrium constant of acetylene is much larger than the equilibrium constant of ethylene. This is consistent with the IR results in Fig. 7, where the IR spectrum following the adsorption of $C_2H_2 + C_2H_4$ mixture on PdAg/β-zeolite is very similar to the adsorption spectrum of pure acetylene. In contrast to the γ-Al_2O_3-supported catalysts, the reaction rate on the PdAg/β-zeolite is lower than Pd/β-zeolite and PdNi/β-zeolite. This may be due to the strong chemisorption of acetylene on the PdAg/β-zeolite. This explanation is also supported by the IR spectra of adsorption on PdAg/γ-Al_2O_3 and PdAg/β-zeolite (Figs. 5 and 6), which show that the IR intensities of adsorbed species are much greater on PdAg/β-zeolite than on PdAg/γ-Al_2O_3.

It is interesting to note that the selectivity for acetylene hydrogenation is about 50% higher on PdNi/β-zeolite than on Pd/β-zeolite, whereas the selectivity for PdNi/γ-Al_2O_3 and Pd/γ-Al_2O_3 are similar. Because the ratio of equilibrium constants, which is dominated by zeolite support, on PdNi/β-zeolite is similar to that on Pd/β-zeolite, the selectivity difference is most likely resulting from a difference in the rate constants for acetylene and ethylene hydrogenation, which is dominated by active metal particles. This supports our point of view that the bimetallic effects resulting from alloying Pd with Ni reduces the rate constant of ethylene more than that of acetylene, as is shown in Table 3. In this case, the bimetallic effects and support effects work together to enhance the catalyst selectivity toward acetylene hydrogenation without any significant loss in activity.

4.3. Comparison with previous results

Previous studies of the selective hydrogenation of acetylene have focused on low loading (0.038–3 wt%) Pd-based catalysts [2,6,8,43,45]. Recently, emphasis has been on tuning catalyst selectivity by the formation of alloys, especially alloying with Ag [44,51–53]. It has been found that alloying with Ag enhances the selectivity of acetylene hydrogenation reaction but decreases the activity. Heinrichs et al. [54] and Lambert et al. [55] observed the same trend for the selective hydrodechlorination of 1,2-dichloroethane into ethylene over Pd–Ag/SiO_2 catalysts. Zhu et. al. [44] found that on 3 wt% Pd/Al_2O_3, the conversion of acetylene reaches 100% at 325.5 K with a negative selectivity of −4%, with the definition of

$$S = \frac{\text{increase of ethylene}}{\text{decrease of acetylene}} \times 100\%,$$

in a flow reactor system [44]. The conversion of acetylene over 3 wt% Pd–6 wt% Ag/Al_2O_3 reaches 100% at 378 K with a selectivity of 38%, much higher than that over Pd/Al_2O_3 catalyst. Another study found that the selectivity of acetylene hydrogenation is 45% on a 0.45 wt% Pd/Stöber silica sphere at 333 K and 80% on a 0.45 wt% Pd–0.25 wt% Ag/Stöber silica sphere when both catalysts are reduced at 773 K [56]. To the best of our knowledge, the effect of adding Ni as a promoter has not yet been reported.

In this paper, we studied the bimetallic effects of alloying Pd with Ag or Ni. Consistent with reports in the literature, we found that alloying Pd with Ag enhances the hydrogenation selectivity in a batch reactor. Our study also shows that alloying Ni reduces the rate constant (k) for ethylene hydrogenation more than acetylene, whereas the equilibrium constants (K) exhibit the opposite trend (Table 3), which leaves room for using support effects to control the relative concentrations of adsorbed acetylene and ethylene.

Most previous studies have been performed on Al_2O_3 or SiO_2 supports [5,6,44,46,52]; there are few studies on the effects of supports, such as pumice [57,58] and zeolite [15]. Duca et al. [57] found that pumice-supported Pd catalysts exhibited good activity and excellent selectivity and stability in the selective hydrogenation of acetylene. Weiss et al. [15] concluded that the reaction rates and selectivity for Pd on silicalite and Pd incorporated into ZSM-5 during synthesis compared favorably with those of a commercial reference catalyst. In the present study, we investigated the support effects of Na^+-exchanged β-zeolite compared with traditional Al_2O_3 supports. We found that the cation–π interaction between Na^+ and acetylene or ethylene helps the catalysts selectively adsorb acetylene over ethylene, so that the selectivity on the Na^+-exchanged β-zeolite-supported catalysts is enhanced compared with the γ-Al_2O_3 counterparts. In particular, PdAg/Na^+-β-zeolite has the highest selectivity of the catalysts studied in the present work. It has also been found that aided by competitive adsorption of the Na^+-exchanged β-zeolite supports, PdNi/Na^+-β-zeolite shows 30% higher selectivity than Pd/Na^+-β-zeolite but maintains similar activity. Moreover, the β-zeolite-supported catalysts have higher dispersions than the γ-Al_2O_3-supported catalysts, leading to an increase in the overall reaction rate in the batch reactor system.

It is widely reported in the literature that the adsorption of acetylene should be stronger than that of ethylene on Pd surfaces. This is consistent with the equilibrium constant (K_1 and K_2) values for the adsorption of acetylene and ethylene on zeolite-supported Pd (Table 3). However, such a trend is not observed in the K values on alumina-supported Pd. This is most likely due to the involvement of the alumina substrate in the competitive adsorption of acetylene and ethylene. As reported

in the literature, there are three types of active sites for the hydrogenation of the acetylene–ethylene mixture on alumina-supported Pd [59,60]. A_1 and A_2 sites are highly selective in the hydrogenation of acetylene to ethylene via a mechanism involving the competitive (A_1) and noncompetitive (A_2) adsorption of acetylene and hydrogen. The E sites are active only for the hydrogenation of ethylene, with both acetylene and ethylene competitively adsorbing on the E sites. Furthermore, on γ-Al_2O_3-supported Pd, ethylene can be hydrogenated on the γ-Al_2O_3 support by means of hydrogen spilled over from Pd [59,61–63]. In this case, the E sites are as important as A sites and play an important role in the selective hydrogenation of acetylene in ethylene. Compared with the active Pd metal sites, the support sites are more abundant with the catalyst loadings used in the present study. As a result, the adsorption of ethylene could be stronger than that of acetylene by involving the support, because the equilibrium constants in Table 3 include contributions from both Pd metals and the γ-Al_2O_3 support.

5. Conclusion

Novel selective hydrogenation catalysts have been synthesized and evaluated using an FTIR batch reactor. The results show that among the γ-Al_2O_3-supported catalysts, the PdAg catalyst has the highest selectivity, whereas PdNi behaves similar to the Pd monometallic catalyst. Preferential adsorption of acetylene over ethylene on Na^+-β-zeolites increases the surface concentration of acetylene, resulting in a further increase in the hydrogenation selectivity of acetylene. Finally, the PdAg/Na^+-β-zeolite catalyst shows significantly higher selectivity than the other catalysts.

Acknowledgments

Financial support was provided by from the US Department of Energy, Office of Science, Division of Chemical Sciences (Grant FG02-03ER15468).

References

[1] J.H. Kang, E.W. Shin, W.J. Kim, J.D. Park, S.H. Moon, Catal. Today 63 (2000) 183–188.
[2] N.S. Schbib, M.A. Garcia, C.E. Gigola, A.F. Errazu, Ind. Eng. Chem. Res. 35 (1996) 1496–1505.
[3] P. Praserthdam, S. Phatanasri, J. Meksikarin, Catal. Today 63 (2000) 209–213.
[4] W.J. Kim, J.H. Kang, I.Y. Ahn, S.H. Moon, Appl. Catal. A 268 (2004) 77–82.
[5] H. Molero, B.F. Bartlett, W.T. Tysoe, J. Catal. 181 (1999) 49–56.
[6] A. Sarkany, A. Beck, A. Horvath, Z. Revay, L. Guczi, Appl. Catal. A 253 (2003) 283–292.
[7] B.M. Choudary, M.L. Kantam, N.M. Reddy, K.K. Rao, Y. Haritha, V. Bhaskar, F. Figueras, A. Tuel, Appl. Catal. A 181 (1999) 139–144.
[8] H.R. Aduriz, P. Bodnariuk, M. Dennehy, C.E. Gigola, Appl. Catal. 58 (1990) 227–239.
[9] S.G. Podkolzin, R. Alcala, J.A. Dumesic, J. Mol. Catal. A Chem. 218 (2004) 217–227.
[10] P.A. Sheth, M. Neurock, C.M. Smith, J. Phys. Chem. B 107 (2003) 2009–2017.
[11] J.W. Medlin, M.D. Allendorf, J. Phys. Chem. B 107 (2003) 217–223.
[12] H. Nakatsuji, M. Hada, T. Yonezawa, Surf. Sci. 185 (1987) 319–342.
[13] J. Horiuchi, M. Polanyi, Trans. Faraday Soc. 30 (1934) 1164–1172.
[14] R.D. Cortright, S.A. Goddard, J.E. Rekoske, J.A. Dumesic, J. Catal. 127 (1991) 342–353.
[15] W.L. Kranich, A.H. Weiss, Z. Schay, L. Guczi, Appl. Catal. 13 (1985) 257–267.
[16] D.R. Corbin, L. Abrams, C. Bonifaz, J. Catal. 115 (1989) 420–429.
[17] D.A. Dougherty, Science 271 (1996) 163–168.
[18] R.I. Keir, D.W. Lamb, G.L.D. Ritchie, J.N. Watson, Chem. Phys. Lett. 279 (1997) 22–28.
[19] T. Kar, R. Ponec, A.B. Sannigrahi, J. Phys. Chem. A 105 (2001) 7737–7744.
[20] N.A. Khan, H.H. Hwu, J.G. Chen, J. Catal. 205 (2002) 259–265.
[21] H.H. Hwu, J. Eng, J.G. Chen, J. Am. Chem. Soc. 124 (2002) 702–709.
[22] N.A. Khan, L.E. Murillo, Y.Y. Shu, J.G. Chen, Catal. Lett. 105 (2005) 233–238.
[23] J.R. Kitchin, J.K. Norskov, M.A. Barteau, J.G. Chen, Phys. Rev. Lett. 93 (2004) 156801.
[24] N.A. Khan, J.G. Chen, in: Nanotechnology in Catalysis, vol. 1, 2004, pp. 17–32.
[25] M.B. Zellner, A.M. Goda, O. Skoplyak, M.A. Barteau, J.G. Chen, Surf. Sci. 583 (2005) 281–296.
[26] B. Hammer, J.K. Norskov, in: Advances in Catalysis, vol. 45, 2000, pp. 71–129.
[27] L.E. Murillo, N.A. Khan, J.G. Chen, Surf. Sci. 594 (2005) 27–42.
[28] S. Lambert, C. Cellier, P. Grange, J.P. Pirard, B. Heinrichs, J. Catal. 221 (2004) 335–346.
[29] C.L.M. Joyal, J.B. Butt, J. Chem. Soc. Faraday Trans. I 83 (1987) 2757–2764.
[30] V. Ponec, G.C. Bond, Catalysis by Metals and Alloy, Elsevier, Amsterdam, 1995.
[31] Y. Somanoto, W.M. Sachtler, J. Catal. 32 (1974) 315–324.
[32] D. Cormack, J. Pritchard, R.L. Moss, J. Catal. 37 (1975) 548–552.
[33] B. Heinrichs, F. Noville, J.P. Schoebrechts, J.P. Pirard, J. Catal. 192 (2000) 108–118.
[34] W.M.H. Sachtler, Catal. Rev. Sci. Eng. 14 (1976) 193–210.
[35] A. Balerna, G. Deganello, L. Liotta, A. Longo, A. Martorana, C. Meneghini, S. Mobilio, A.M. Venezia, J. Non-Cryst. Solids 293 (2001) 682–687.
[36] J.M. Wei, E. Iglesia, J. Catal. 224 (2004) 370–383.
[37] M.C.J. Bradford, M.A. Vannice, Appl. Catal. A 142 (1996) 97–122.
[38] H. Yang, J.L. Whitten, J. Chem. Phys. 98 (1993) 5039–5049.
[39] D.J. Moon, M.J. Chung, K.Y. Park, S.I. Hong, Appl. Catal. A 168 (1998) 159–170.
[40] P. Basu, T.H. Ballinger, J.T. Yates, Rev. Sci. Instrum. 59 (1988) 1321–1327.
[41] R. Kramer, Chemometric Techniques for Quantitative Analysis, Dekker, New York, 1998.
[42] A.B. Mhadeshwar, J.R. Kitchin, M.A. Barteau, D.G. Vlachos, Catal. Lett. 96 (2004) 13–22.
[43] J. Gislason, W.S. Xia, H. Sellers, J. Phys. Chem. A 106 (2002) 767–774.
[44] Q.W. Zhang, J. Li, X.X. Liu, Q.M. Zhu, Appl. Catal. A 197 (2000) 221–228.
[45] C.E. Gigola, H.R. Aduriz, P. Bodnariuk, Appl. Catal. 27 (1986) 133–144.
[46] R.K. Nandi, P. Georgopoulos, J.B. Cohen, J.B. Butt, R.L. Burwell, D.H. Bilderback, J. Catal. 77 (1982) 421–431.
[47] S. Shaikhutdinov, M. Heemeier, M. Baumer, T. Lear, D. Lennon, R.J. Oldman, S.D. Jackson, H.J. Freund, J. Catal. 200 (2001) 330–339.
[48] P.S. Cremer, G.A. Somorjai, J. Chem. Soc. Faraday Trans. 91 (1995) 3671–3677.
[49] P.S. Cremer, X.C. Su, Y.R. Shen, G.A. Somorjai, J. Am. Chem. Soc. 118 (1996) 2942–2949.
[50] T. Miura, H. Kobayashi, K. Domen, J. Phys. Chem. B 104 (2000) 6809–6814.
[51] D.C. Huang, K.H. Chang, W.F. Pong, P.K. Tseng, K.J. Hung, W.F. Huang, Catal. Lett. 53 (1998) 155–159.
[52] R.N. Lamb, B. Ngamsom, D.L. Trimm, B. Gong, P.L. Silveston, P. Praserthdam, Appl. Catal. A 268 (2004) 43–50.

[53] G. Meitzner, J.H. Sinfelt, Catal. Lett. 30 (1995) 1–10.
[54] B. Heinrichs, J.P. Schoebrechts, J.P. Pirard, J. Catal. 200 (2001) 309–320.
[55] S. Lambert, F. Ferauche, A. Brasseur, J.P. Pirard, B. Heinrichs, Catal. Today 100 (2005) 283–289.
[56] Y.M. Jin, A.K. Datye, E. Rightor, R. Gulotty, W. Waterman, M. Smith, M. Holbrook, J. Maj, J. Blackson, J. Catal. 203 (2001) 292–306.
[57] D. Duca, F. Frusteri, A. Parmaliana, G. Deganello, Appl. Catal. A 146 (1996) 269–284.
[58] D. Duca, F. Arena, A. Parmaliana, G. Deganello, Appl. Catal. A 172 (1998) 207–216.
[59] A. Borodzinski, A. Golebiowski, Langmuir 13 (1997) 883–887.
[60] A. Borodzinski, A. Cybulski, Appl. Catal. A 198 (2000) 51–66.
[61] A. Sarkany, L. Guczi, A.H. Weiss, Appl. Catal. 10 (1984) 369–388.
[62] S. Leviness, V. Nair, A.H. Weiss, Z. Schay, L. Guczi J. Mol. Catal. 25 (1984) 131–140.
[63] A. Borodzinski, Pol. J. Chem. 69 (1995) 111–117.
[64] A.V. Kiselev, V.I. Lygin, Infrared Spectra of Surface Compounds, Wiley, New York/Toronto, 1975.
[65] B.E. Bent, Chem. Rev. 96 (1996) 1361–1390.
[66] T.P. Beebe, J.T. Yates, J. Phys. Chem. 91 (1987) 254–257.
[67] S.S. Randhava, A. Rehmat, Trans. Faraday Soc. 66 (1) (1970) 235–241.
[68] M.P. Lapinski, J.G. Ekerdt, J. Phys. Chem. 94 (1990) 4599–4610.